Application Note

Cancer Biology

Agilent

Trusted Answers

Expression and Intracellular Translocation of Cancer Biomarkers in Hepatocarcinoma Cells Induced by Changes in Mitochondrial Metabolism

Authors

Brad Larson
Agilent Technologies, Inc.

Monika Gooz and Eduardo N. Maldonado
Drug Discovery and Biomedical Sciences, Medical University of South Carolina

Abstract

Hepatocarcinoma is one of the most common cancer types in the U.S. with limited treatment options and poor survival rate. Recently, cancer bioenergetics emerged as a promising source of targets to develop novel anticancer agents. The identification of relevant biomarkers is essential for screening and validation of small molecules proposed as chemotherapeutic agents. In this regard, there is a great need for high-throughput/high-content methods, which require short, reproducible sample preparation techniques. This application note utilizes the erastin-like compound X1, which is known to modulate cancer cell bioenergetics, and the well-characterized SNU-449 liver cancer cell line as the model system. As readout, directly and indirectly labeled fluorescent antibodies were employed to visualize and quantify expression of proliferative and antiproliferative markers Ki-67 and cytoskeleton-associated protein 4/p63 (CKAP4/p63), as well as the tumor suppressor protein p53. Using the Agilent BioTek Cytation 5 cell imaging multimode reader and Agilent BioTek Gen5 microplate reader and imager software, these markers and the corresponding antibodies were successfully validated for studying the long-term effect of mitochondrial bioenergetics modulators on cancer cells. This method allows a fast and reliable screening of potential drug candidates for further development.

Introduction

Liver cancer is the sixth-most common cancer, with an incidence three times higher in men than women. Hepatocellular carcinoma (HCC) accounts for 73% of hepatic cancers. The American Cancer Society estimates that 41,000 new liver cancer cases will be diagnosed, and more than 30,000 people will die from this disease in 2022.[1] Nonpharmacological treatments include surgery, embolization, and transplantation. Patients diagnosed in the early stages of liver cancer may benefit from targeted immunotherapy. However, the five-year survival rate of HCC patients is only 35%. Recently, targeting cancer cell bioenergetics was identified as a promising, novel therapeutic option.[2,3]

Rapidly proliferating tumor cells require metabolic adaptations to cope with the demands of frequent cell divisions. Cancer cells in general display the Warburg effect, characterized by enhanced aerobic glycolytic activity and partial suppression of mitochondrial metabolism.[4,5] In mammalian cells, mitochondria are the main energy-producing organelles that contribute to cellular ATP level through oxidative phosphorylation. Most of the metabolites utilized by mitochondria enter the organelles through voltage-dependent anion channels (VDAC) located in the outer mitochondrial membrane. Interestingly, there is increasing evidence that, depending on the type of cancer, the contribution of glycolytic and mitochondrial metabolic pathways to the cellular ATP pool varies and, in some of them, oxidative metabolism is prevalent over glycolysis.

Mitochondria are involved not only in cellular metabolism but also in important interactions between cytoplasmic, endoplasmic reticulum (ER), and mitochondrial proteins, which regulate cell survival and apoptosis.[6] VDAC opening or closing has been proposed to regulate the flux of metabolites between mitochondria and the cytosol, operating as a switch to regulate cancer cell metabolism.[7–9] Previously, free intracellular tubulin was shown to bind to and close the channel.[8,10] The small molecules erastin and erastin-like X1 were identified as antagonists of the VDAC–tubulin interaction. Blocking of the inhibitory effect of free tubulin on VDAC resulted in increased mitochondrial metabolism, reactive oxygen species (ROS) formation, mitochondrial dysfunction, and cell death in hepatocarcinoma cells.[11]

Successful solid tumor treatment results from both inhibition of cell proliferation and drug-induced cancer cell death. The nuclear protein Ki-67, expressed during the G_1 phase of the cell cycle, is widely used as a cell proliferation marker in tissue biopsies to predict treatment efficiency.[12] It is also utilized to predict the effect of drugs or drug combinations ex vivo[13,14], antigen-specific T cell proliferation in vitro[15], or the proliferative potential of cancer cells in culture. CKAP4/p63 is located in the ER and was identified as a high-affinity receptor for the antiproliferative factor.[16,17] The role of CKAP4 in HCC is controversial. The receptor was reported to inhibit growth and metastasis of HCC cells in culture as well as in a xenograft mouse model of HCC.[18] Further, high circulating CKAP4 levels in HCC patients versus patients with chronic hepatitis B or cirrhosis was observed.[19] Proteomics analysis identified upregulated CKAP4 in tumor tissue of HCC patients with microvasculature invasion.[20] Another study found higher overall and disease-free survival rate in HCC patients with higher CKAP4 expression compared to patients with lower levels of the receptor.[18] However, some contradicting data exist.[21]

The p53 tumor suppressor protein is widely regarded as the transcription factor that activates DNA repair mechanisms and provides genomic stability through cell cycle regulation. The loss of p53 activity through mutations has been found in many malignant tumors.[22,23] However, p53 also has extranuclear functions including the regulation of cellular metabolism, apoptosis, necrosis, and autophagy.[24] There is increasing evidence that upon cellular stress (e.g., increase in ROS or DNA damage), the p53 protein translocates to the mitochondria and interacts directly with both anti-apoptotic and pro-apoptotic Bcl-2 protein family members, inducing p53-dependent apoptosis.[24] There is some evidence that p53 can also indirectly induce apoptosis by promoting GSKβ-dependent phosphorylation of VDAC1.[25] In cancer cells, mutated p53 promotes glucose uptake. In addition, if there is ATP shortage, it induces aerobic glycolysis (Warburg effect) and favors lipid metabolism. Wild type p53 also has an important role in suppressing cellular ROS formation to preserve cellular integrity. However, mutated p53 promotes a higher level of oxidants, which contributes to DNA mutations, cancer cell hyperproliferation, and thus tumor survival.[23]

The current study characterizes the effect of the erastin-like compound X1 on proliferative and antiproliferative markers that could be utilized as cancer biomarkers during drug discovery. Anti-Ki67, anti-CKAP4, and anti-p53 antibodies were used, which were previously mostly utilized for tissue immunostaining protocols, and validated for high-content screening using SNU-499 liver cancer cells using the Cytation 5 cell imaging multimode reader.

Experimental

Materials

Agilent Dako antibodies

Monoclonal mouse anti-human Ki-67 antigen/FITC, clone MIB-1 (part number F726801-1), monoclonal mouse anti-human plasma cell/PerCP-Cy5.5, clone VS38c (part number PR71350-1), monoclonal mouse anti-human p53 protein, clone DO-7, unconjugated (part number M700101-2), polyclonal goat anti-mouse immunoglobulins/RPE. Affinity-isolated F(ab')2 (part number R048001-2), and mouse IgG1/FITC (part number X092701-5) were donated by Agilent Dako (Glostrup, Denmark).

Other experimental components

Hoechst 34580 (part number 63493) was purchased from Sigma-Aldrich (St. Louis, MO, U.S.). Alexa Fluor 488 phalloidin (part number A12379) was purchased from Thermo Fisher Scientific (Waltham, MA, U.S.). X1 compound[11] was previously identified from the MUSC ChemBridge DIVERSet library. Bovine serum albumin (BSA; part number A7030) and DMSO (part number 67685) were purchased from Sigma**,** and phosphate buffered saline (PBS; part number 10010072) was from Thermo Fisher Scientific. CELLview cell culture slides, PS, 75/25 mm, glass bottom, 10 compartments, TC, sterile (part number 543079) were donated by Greiner Bio-One North America (Monroe, NC, U.S.).

Agilent BioTek Cytation 5 cell imaging multimode reader

The Cytation 5 is a modular multimode microplate reader combined with an automated digital microscope. Filter- and monochromator-based microplate reading are available, and the microscopy module provides up to 60x magnification in fluorescence, brightfield, color brightfield, and phase contrast. The instrument can perform fluorescence imaging in up to four channels in a single step. With special emphasis on live cell assays, the Cytation 5 features shaking, temperature control to 65 ºC, CO_2/O_2 gas control, and dual injectors for kinetic assays. It is controlled by integrated Gen5 microplate reader and imager software, which also automates image capture, analysis, and processing. The Cytation 5 was used to image the immunostained SNU-449 cells following X1 compound treatment.

Methods

Cell propagation and cell culture slide plating

Cells

SNU-449 human hepatocellular carcinoma cells (part number CRL-2234), were obtained from the American Tissue Culture Collection (ATCC, Manassas, VA, U.S.). Cells were cultured in RPMI-1640 medium supplemented with 10% fetal bovine serum (FBS) premium from Atlanta Biologicals (Flowery Branch, GA, U.S.), 100 unit/mL penicillin, and 100 µg/mL streptomycin in 5% CO_2/air at 37 °C.

X1 compound treatment

SNU-449 cells (25,000/well) were plated into glass bottom 10-compartment tissue culture (TC)-treated CELLview slides (Greiner Bio One, part number 543079). The following day, cells were treated with either 10 µM X1 compound or vehicle (DMSO) for 48 hours.

Immunofluorescent staining protocol

After 48-hour treatment with 10 µM X1 compound or vehicle, SNU-449 cells were gently washed in PBS, fixed with 2% paraformaldehyde for 10 minutes, and permeabilized with 0.1% Triton-X 100 in PBS for 10 minutes. Nonspecific antigen sites were blocked with 1% BSA for 30 to 60 minutes. Samples were incubated with a 1:100 dilution of appropriate primary antibodies in 1% BSA overnight at 4 °C. The following day, the unlabeled monoclonal mouse anti-human p53 antibody and the unlabeled mouse IgG1 treated samples were washed in PBS and incubated with a 1:1000 dilution of the RPE-labelled goat anti-mouse antibody at room temperature for one hour. All samples were washed in PBS and appropriate samples were incubated with 1:1000 dilution of fluorescent-labelled phalloidin in 1% BSA for 1 hour (see the "Results and discussion" section). To label nuclei, cells were incubated with 1:5000 dilution of Hoechst (Thermo Fisher Scientific, part number H3570) for 5 minutes and washed in PBS.

Cancer biomarker fluorescent probe imaging

Following completion of the immunostaining protocol, the CELLview slide was placed onto the Agilent BioTek two-position slide adapter (part number 1220548) and inserted into the Cytation 5 for imaging. Table 1 lists the settings used to image the sample wells on each slide.

Table 1. Summary of imaging channel combinations.

Cancer Biomarker Fluorescent Imaging Channel Combinations		
Ki-67/VS38c		
Ki-67	Monoclonal mouse anti-human Ki-67 antigen/FITC, clone MIB-1	GFP
VS38c	Monoclonal mouse anti-human plasma cell/PerCP-Cy5.5, clone VS38c	CY5.5
Nuclear Probe	Hoechst 34580	DAPI
p53		
p53	Polyclonal goat anti-mouse immunoglobulins/RPE. Affinity-isolated F(ab')2	RFP
Actin Probe	Alexa Fluor 488 phalloidin	GFP
Nuclear Probe	Hoechst 34580	DAPI
IgG Negative Control		
	Mouse IgG1/FITC	GFP
Nuclear Probe	Hoechst 34580	DAPI

A combination of 20x and 40x images were captured from each test well. The 20x images were captured at a single Z-plane, while the 40x images incorporated a 10-step Z-stack, with images being captured every 0.8 µm, to ensure each cell within the field of view was imaged in focus.

Image processing

A background removal step was then applied to all images (Table 2). This served to remove background signal and increase the sensitivity of the cellular analysis algorithm for proper mask placement.

Table 2. Image background signal removal parameters.

Background Removal Parameters								
	20x Ki-67/IgG Negative Control		**40x Ki-67/VS38c**			**40x p53**		
	DAPI	GFP	DAPI	GFP	CY5.5	DAPI	GFP	RFP
Background	Dark							
Rolling Ball Diameter	138 µm	15 µm	25 µm	6 µm	70 µm	85 µm	138 µm	15 µm
Image Smoothing Strength	0							

Deconvolution was also performed to sharpen the boundaries of each cellular compartment to be analyzed (Table 3).

Table 3. Image deconvolution parameters.

Deconvolution Parameters			
	20x Ki-67/IgG Negative Control	**40x Ki-67/VS38c**	**40x p53**
Standard Deviation	0.806	**3**	2
Kernel Radius	2	**13**	9
Iterations	5		

A single image projection was then created from the 10-slice stitched Z-stack (Table 4). The focus stacking method was chosen, which automatically selects the most in-focus pixel from each image in the stack for inclusion in the final projection. This combination of image-processing algorithms allows the most accurate analysis of each final image.

Table 4. Image Z-projection parameters.

Z-Projection Parameters	
Method	Focus stacking
Size of Maximum Filter	11 px
Z-Slices Included	All slices

Cellular analysis of Ki-67 and VS38c expression

Following image processing, quantification of Ki-67, VS38c, and p53 expression was carried out using the 40x images and the criteria explained in Table 5.

Table 5. Cellular analysis parameters.

Primary Cellular Analysis		
Criteria	**Ki-67/VS38c**	**p53**
Channel	ZProj[Deconvolved[Tsf[DAPI 377,447]]]	
Threshold	3,000	5,000
Background	Dark	
Split Touching Objects	Checked	
Fill Holes in Masks	Checked	
Minimum Object Size	5	
Maximum Object Size	40	100
Include Primary Edge Objects	Checked	
Analyze Entire Image	Checked	
Rolling Ball Diameter	25	Auto
Image Smoothing Strength	2	
Evaluate Background On	5	
Secondary Cellular Analysis		
Criteria	**Ki-67/VS38c**	**p53**
Channel	ZProj[Deconvolved[Tsf [GFP 469,525]]]	ZProj[Deconvolved[Tsf[RFP 531,593]]]
Measure Within a Primary Mask	Checked (use primary mask)	
Channel	ZProj[Deconvolved[Tsf [CY5.5 647,794]]]	ZProj[Deconvolved[Tsf[RFP 531,593]]]
Measure Within a Secondary Mask	Checked	
Type	Exclude primary mask	
Distance from Primary Mask	0	
Ring Width	25	40
Threshold	5,000	4,000
Smooth	2	4
Method	Propagate mask	Threshold in mask
Fill Holes in the Mask	Unchecked	
Evaluate Background On	5	

Calculated Metrics of Interest		
Metric of Interest	Object Mean[Deconvolved [Tsf[GFP 469,525]]]	Object Area[ZProj [Deconvolved[Tsf[RFP 531,593]]]]
Metric of Interest	Object Mean_2 [Deconvolved[Tsf[CY5.5 647,794]]]	Object Area_2[ZProj [Deconvolved[Tsf[RFP 531,593]]]]
Metric of Interest		Object Area_2[ZProj [Deconvolved[Tsf[RFP 531,593]]]] / Object Area[ZProj[Deconvolved [Tsf[RFP 531,593]]]]

Results and discussion

Confirmation of antigen-specific IgG antibody binding

To ensure that fluorescence from immunostained cells was due to specific antibody binding to the target antigen, an initial test was performed using a nonspecific negative control antibody. As each of the antigen-specific antibodies to be used were IgG, a FITC-labeled IgG1 negative control antibody was tested in the SNU-449 HCC cells, along with a Ki-67-specific antibody, to compare binding rates in addition to the fluorescent signal.

The images taken of SNU-449 cells following immunostaining with the Ki-67 specific proliferation marker antibody demonstrate a higher level of FITC signal captured in the GFP channel compared to immunostaining with the IgG1 negative control antibody (Table 6). This confirmatory experiment assured that signal from subsequent experiments resulted from the binding of the antibody to target antigens.

Table 6. Agilent Dako IgG antibody binding images: 20x images of SNU-449 cells following immunostaining with Ki-67-specific antibody, or IgG1 negative control antibody.

	Anti-Human Ki-67 Antigen/FITC Antibody	**Mouse IgG1/FITC Negative Control Antibody**
DAPI/GFP Overlaid Image	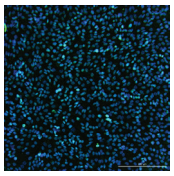	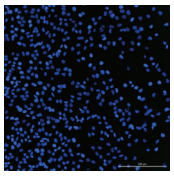
GFP Image Only	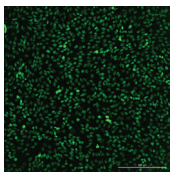	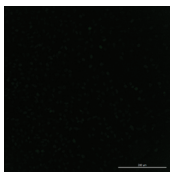

Ki-67 and CKAP4/p63 biomarker expression analysis

Following confirmation of antibody-specific binding, experiments were performed to determine the effect of the X1 compound on expression of three separate biomarkers: the proliferation marker Ki-67, the antiproliferative marker CKAP4/p63, and the tumor suppressor protein p53. In the first experiment, the effect on Ki-67 and CKAP4/p63 was assessed. Upon completion of the 48-hour incubation with the X1 compound, immunostaining was carried out as previously explained, with the addition of the anti-human Ki-67 antigen and anti-human plasma cell clone VS38c antibodies. Anti-Ki67 antibody recognizes the Ki-67 nuclear protein, while the anti-VS38c antibody recognizes the cytoskeleton-linking membrane protein 63 (CKAP4/p63 receptor) present in the rough ER. Therefore, increased antibody binding is indicative of increased Ki-67 and CKAP4/p63 expression, respectively. Images were captured using a 40x objective and fluorescent imaging channels, as explained in Table 1.

The 40x images were visualized to assess whether X1 affected Ki-67 or CKAP4/p63 expression. Images in Figure 1 show that the FITC signal from the labeled anti-Ki-67 antibody is higher in the vehicle control compared to X1-treated cells. The opposite can be seen for the anti-VS38c antibody compared to the vehicle control. CKAP4/p63 expression increased after incubation with X1.

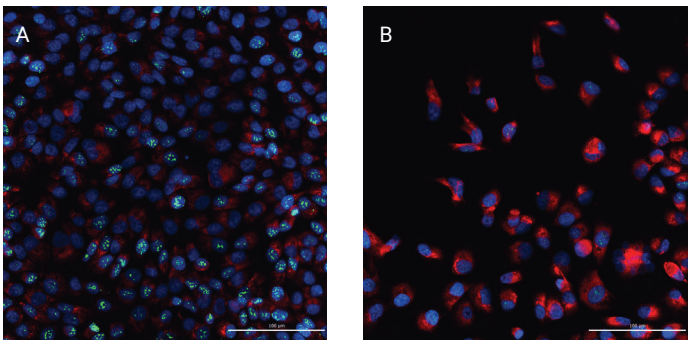

Figure 1. The 40x images demonstrating Ki-67 and CKAP4/p63 expression following 48-hour incubation with (A) vehicle (negative control), or (B) 10 µM X1 compound treatment.

Changes in biomarker expression were then quantified again using the cellular analysis tools of Gen5, and the criteria detailed in Table 5. Since Ki-67 is localized in the nuclear compartment, primary masks were placed around each nucleus that was captured within the image, using signal from the Hoechst 34580 probe captured in the DAPI channel. A secondary mask was then created around the previously placed primary masks for CKAP4/p63, as this biomarker is localized in the cytoplasm. This was done by extending out a ring from the boundary of the primary mask that was sufficient to include all the signal from the CY5.5-labeled VS38c antibody; in this case, 25 µm.

The average signal from bound FITC-labeled Ki-67 antibody, captured in the GFP channel within each primary mask, as well as the average signal from the bound CY5.5-labeled VS38c antibody, captured in the CY5.5 channel within the corresponding cytoplasmic area, following treatment with X1 or with negative control, was then plotted (Figure 2).

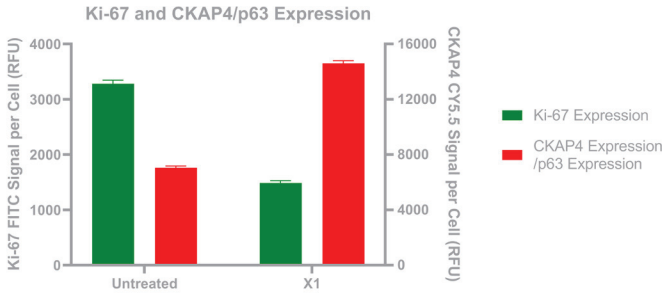

Figure 2. Quantified Ki-67 and CKAP4/p63 biomarker signal following X1 compound treatment; n = 597 untreated and 541 treated cells analyzed.

The results of the experiment demonstrate that X1 negatively affects the proliferative ability and viability of the SNU-449 cells. This agrees with previously published results showing that X1 modulates cancer cells bioenergetics, decreases glycolysis, increases mitochondrial metabolism, and promotes cancer cell death through increased ROS generation.[11,26,27]

p53 biomarker expression analysis

Following analysis of proliferative and antiproliferative markers, expression of the tumor-suppressor protein p53 was analyzed. Upon completion of the four-hour incubation with X1, immunostaining was performed as described previously.

The unconjugated mouse anti-human p53 protein antibody, followed by the polyclonal goat anti-mouse RPE-labeled antibody, were added. The signal captured in the RFP channel was indicative of localized p53 expression. The images were again captured using a 40x objective and the fluorescent imaging channels, as explained in Table 1.

The anti-p53 antibody recognizes the transcription factor p53, which is present in the nucleus. However, upon visualization of the captured 40x images, it was seen that p53 expression also appeared in the cytoplasm following treatment with X1 (Figure 3).

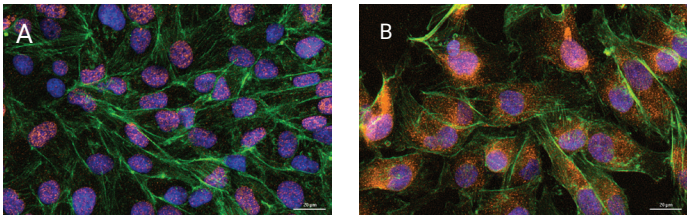

Figure 3. p53 expression following 48-hour incubation with (A) vehicle (negative control), or (B) X1 (10 µM).

The cellular analysis tools within Gen5 were then used to quantify p53 translocation. Initially, a primary mask was placed around each nucleus captured within the image to determine expression within the nuclear compartment. The Hoechst 33342 signal, captured in the DAPI channel, was again used, in addition to criteria explained in Table 5. As p53 expression translocated from the nuclear compartment upon treatment with X1, a secondary mask was set to quantify the extent of movement into the cytoplasm. This was done by extending a ring out from the boundary of the primary mask that was sufficient to include all the signal from the RPE-labeled antibody, as explained previously for the CKAP4/p63 biomarker; in this case, 35 µm. A threshold in the RFP channel was then set to only include areas of positive signal indicating p53 expression.

The area from the nuclear compartment within each primary mask counted, as well as the area of cytoplasmic p53 expression within the secondary mask were then quantified. This was done for untreated wells, in addition to those treated with 10 µM X1 (Figure 4, left Y-axis). The ratio of cytoplasmic to nuclear area for each cell was also calculated (Figure 4, right Y-axis).

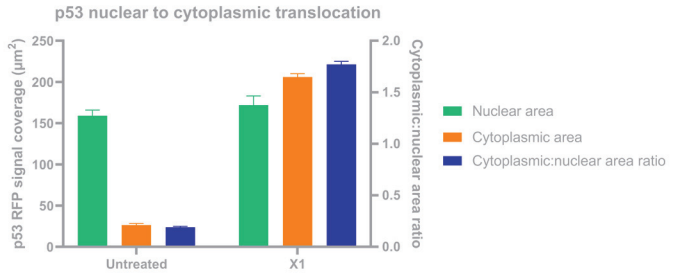

Figure 4. Analysis of p53 biomarker translocation. Quantification of signal from 40x images within nuclear and cytoplasmic cellular compartments, as well as a normalized cytoplasmic:nuclear signal ratio, following treatment with vehicle (negative control); or X1 (10 µM); n = 523 untreated and 602 treated cells analyzed.

Conclusion

The aim of the current application was to develop and validate quantifiable, simple, and fast methods for screening anticancer drug candidates (small molecules) in tumor cell cultures. The model system used was the SNU-449 liver carcinoma cell line. First, changes in the expression of the pro-proliferative marker Ki-67 nuclear protein and the antiproliferative marker CKAP4/p63 ER receptor were measured. In a second application, changes in expression and localization of the tumor suppressor p53 were evaluated. Since the translocation of p53 from the nucleus to the cytoplasm and organelles like mitochondria is suggested to promote cell death, quantitative analysis of this event can be an additional, important tool for drug discovery. Through the inclusion of multiple biomarkers, it was confirmed that the X1 compound has antiproliferative properties in SNU-499 hepatocarcinoma cells as well, confirming previous findings.[11,26,27] Further, it was observed that the X1 compound promotes p53 translocation, which opens new avenues in investigating its effect in cancer cell death. Finally, by combining immunofluorescent staining with the imaging capabilities of the Agilent BioTek Cytation 5 cell imaging multimode reader and sample analysis features of the Agilent BioTek Gen5 microplate reader and imager software, an easy-to-use, robust method to evaluate the effect of mitochondrial bioenergetics modulation on cancer biomarkers expression and intracellular translocation in hepatocarcinoma cells was created.

References

1. American Cancer Society. *Cancer Facts and Figures 2022.* Atlanta: American Cancer Society, **2022**. https://www.cancer.org/content/dam/cancer-org/research/cancer-facts-and-statistics/annual-cancer-facts-and-figures/2022/2022-cancer-facts-and-figures.pdf (accessed 2022-10-27).
2. Crunkhorn, S. Cancer: Disrupting Energy Metabolism. *Nat Rev Drug Discov*, **2018**, *17*(10), 708. DOI: 10.1038/nrd.2018.172
3. Wallace, D.C. Mitochondria and Cancer. *Nat Rev Cancer*, **2012**, *12*(10), 685–698. DOI: 10.1038/nrc3365
4. Warburg, O.; Wind, F.; Negelein, E. The Metabolism of Tumors in the Body. *J Gen Physiol*, **1927**, *8*(6), 519–530. DOI: 10.1085/jgp.8.6.519
5. Warburg, O. On the Origin of Cancer Cells. *Science*, **1956**, *123*(3191), 309–314. DOI: 10.1126/science.123.3191.309
6. Marchi, S.; Patergnani, S.; Missiroli, S.; Morciano, G.; Rimessi, A.; Wieckowski, M.R.; Giorgi, C.; Pinton, P. Mitochondrial and Endoplasmic Reticulum Calcium Homeostasis and Cell Death. *Cell Calcium*, **2018**, *69*, 62–72. DOI: 10.1016/j.ceca.2017.05.003
7. Maldonado, E.N. and Lemasters, J.J. Warburg Revisited: Regulation of Mitochondrial Metabolism by Voltage-Dependent Anion Channels in Cancer Cells. *J Pharmacol Exp Ther*, **2012**, *342*(3), 637–641. DOI: 10.1124/jpet.112.192153
8. Maldonado, E.N.; Sheldon, K.L.; DeHart, D.N.; Patnaik, J.; Manevich. Y.; Townsend, D.M.; Bezrukov, S.M.; Rostovtseva, T.K.; Lemasters, J.J. Voltage-Dependent Anion Channels Modulate Mitochondrial Metabolism in Cancer Cells: Regulation by Free Tubulin and Erastin. *J Biol Chem*, **2013**, *288*(17), 11920–11929. DOI: 10.1074/jbc.M112.433847
9. Maldonado, E.N. VDAC-Tubulin, an Anti-Warburg Pro-Oxidant Switch. *Front Oncol*, **2017**, *7*, 4. DOI: 10.3389/fonc.2017.00004
10. Rostovtseva, T.K.; Sheldon, K.L.; Hassanzadeh, E.; Monge, C.; Saks, V.; Bezrukov, S.M.; Sackett, D.L. Tubulin Binding Blocks Mitochondrial Voltage-Dependent Anion Channel and Regulates Respiration. *Proc Natl Acad Sci U S A*, **2008**, *105*(48), 18746–18751. DOI: 10.1073/pnas.0806303105
11. DeHart, D.N.; Lemasters, J.J.; and Maldonado, E.N. Erastin-Like Anti-Warburg Agents Prevent Mitochondrial Depolarization Induced by Free Tubulin and Decrease Lactate Formation in Cancer Cells. *SLAS Discov*, **2018**, *23*(1), 23–33. DOI: 10.1177/2472555217731556
12. Miller, I.; Min, M.; Yang, C.; Tian, C.; Gookin, S.; Carter, D.; Spencer, S.L., Ki67 is a Graded Rather than a Binary Marker of Proliferation versus Quiescence. *Cell Rep*, **2018**, *24*(5), 1105–1112. DOI: 10.1016/j.celrep.2018.06.110
13. Tozuka, K.; Horiguchi, J.; Takata, D.; Rokutanda.; Nagaoka, R.; Tokiniwa, H.; Kikuchi, M.; Satou, A.; Takei, H.; Takeyoshi, I., Collagen Gel Droplet-Embedded Culture-Drug Sensitivity Test and Ki67 Expression in Estrogen Receptor-Positive and HER2-Negative Breast Cancer. *Mol Clin Oncol*, **2013**, *1*(1), 93–99. DOI: 10.3892/mco.2012.4
14. Gianni, L.; Colleoni, M.; Bisagni, G.; Mansutti, M.; Zamagni, C.; Mastro, L.D.; Zambelli, S.; Bianchini, G.; Frassoldati, A.; Maffies, I. et al. Effects of Neoadjuvant Trastuzumab, Pertuzumab, and Palbociclib on Ki67 in HER2 and ER-Positive Breast Cancer. *NPJ Breast Cancer*, **2022**, *8*(1),1. DOI: 10.1038/s41523-021-00377-8
15. Soares, A.; Govender, L.; Hughes, J.; Mavakla, W.; de Kock, M.; Barnard, C.; Pienaar, B.; van Rensburg, E.J.; Jacobs, G.; Khomba, G. et al Novel Application of Ki67 to Quantify Antigen-Specific In Vitro Lymphoproliferation. *J Immunol Methods*, **2010**, *362*(1–2), 43–50. DOI: 10.1016/j.jim.2010.08.007
16. Conrads, T.P; Tocci, G.M.; Hood, B.L.; Zhang, C.O.; Guo, L.; Koch, K.R.; Michejda, C.J.; Veenstra, T.D.; Keay, S.K. CKAP4/p63 is a Receptor for the Frizzled-8 Protein-Related Antiproliferative Factor from Interstitial Cystitis Patients. *J Biol Chem*, **2006**, *281*(49), 37836–37843. DOI: 10.1074/jbc.M604581200
17. Planey, S.L.; Keay, S.K.; Zhang, C.O.; Zacharias, D.A. Palmitoylation of Cytoskeleton Associated Protein 4 by DHHC2 Regulates Antiproliferative Factor-Mediated Signaling. *Mol Biol Cell*, **2009**, *20*(5), 1454–1463. DOI: 10.1091/mbc.E08-08-0849
18. Li, S.X.; Liu, L.J.; Dong, L.W.; Shi, H.G.; Pan, Y.F.; Tan, Y.X.; Zhang, J.; Zhang, B.; Ding, Z.W.; Jiang, T.Y. et al. CKAP4 Inhibited Growth and Metastasis of Hepatocellular Carcinoma Through Regulating EGFR Signaling. *Tumour Biol*, **2014**, *35*(8), 7999–8005. DOI: 10.1007/s13277-014-2000-3
19. Wang, Y.; Yu, W.; Mingging, H.; Huang, Y.; Wang, M.; Zhu, J., Serum Cytoskeleton-Associated Protein 4 as a Biomarker for the Diagnosis of Hepatocellular Carcinoma. *Onco Targets Ther*, **2019**, *12*, 359–364. DOI: 10.2147/OTT.S189425

20. Cao, Y.; Ding, W.W.; Zhang, J.Z.; Gao, Q.; Yag, H.X.; Cao, W.S.; Wang, Z.X.; Fang, L.; Du, R.H. Significant Down-Regulation of Urea Cycle Generates Clinically Relevant Proteomic Signature in Hepatocellular Carcinoma Patients with Macrovascular Invasion. *J Proteome Res*, **2019**, *18*(5), 2032–2044. DOI: 10.1021/acs.jproteome.8b00921
21. Chen, Z.Y.; Wang, T.; Gan, X.; Chen, S.H.; He, Y.T.; Wang, Y.Q.; Zhang, K.H. Cytoskeleton-Associated Membrane Protein 4 is Upregulated in Tumor Tissues and is Associated with Clinicopathological Characteristics and Prognosis in Hepatocellular Carcinoma. *Oncol Lett*, **2020**, *19*(6), 3889–3898. DOI: 10.3892/ol.2020.11499
22. Kruiswijk, F.; Labuschagne, C.F.; Vousden, K.H. p53 in Survival, Death, and Metabolic Health: A Lifeguard with a Licence to Kill. *Nat Rev Mol Cell Biol*, **2015**, *16*(7), 393–405. DOI: 10.1038/nrm4007
23. Haupt, S.; Raghu, D.; Haupt, Y. Mutant p53 Drives Cancer by Subverting Multiple Tumor Suppression Pathways. *Front Oncol*, **2016**, *6*, 12. DOI: 10.3389/fonc.2016.00012
24. Blandino, G.; Valenti, F.; Sacconi, A.; Agostino, S.D. Wild Type^{-} and Mutant p53 Proteins in Mitochondrial Dysfunction: Emerging Insights in Cancer Disease. *Semin Cell Dev Biol*, **2020**, *98*, 105–117. DOI: 10.1016/j.semcdb.2019.05.011
25. Xue, Y.N.; Yu, B.B.; Li, J.L.; Guo, R.; Zhang, L.C.; Sun, L.K.; Liu, Y.N.; Li, Z. Zinc and p53 Disrupt Mitochondrial Binding of HK2 by Phosphorylating VDAC1. *Exp Cell Res*, **2019**, *374*(1), 249–258. DOI: 10.1016/j.yexcr.2018.12.002
26. Fang, D. and Maldonado, E.N. VDAC Regulation: A Mitochondrial Target to Stop Cell Proliferation. *Adv Cancer Res*, **2018**, *138*, 41–69. DOI: 10.1016/bs.acr.2018.02.002
27. DeHart, D.N.; Fang, D.; Heslop, K.; Li, L.; Lemasters, J.J.; Maldonado, E.N. Opening of Voltage Dependent Anion Channels Promotes Reactive Oxygen Species Generation, Mitochondrial Dysfunction and Cell Death in Cancer Cells. *Biochem Pharmacol*, **2018**, *148*, 155–162. DOI: 10.1016/j.bcp.2017.12.022

www.agilent.com/lifesciences/biotek

RA44865.6855324074

Published in the USA, October 27, 2022
5994-5491EN

Agilent
Trusted Answers